Codelivery of an Optimal Drug/siRNA Combination Using Mesoporous Silica Nanoparticles To Overcome Drug Resistance in Breast Cancer *in Vitro* and *in Vivo*

Huan Meng,[†,*] Wilson X. Mai,[†] Haiyuan Zhang,[†] Min Xue,[‡] Tian Xia,[†] Sijie Lin,[†] Xiang Wang,[†] Yang Zhao,[†] Zhaoxia Ji,[§] Jeffrey I. Zink,[‡,§] and Andre E. Nel[†,§]

[†]Division of NanoMedicine, Department of Medicine, [‡]Department of Chemistry & Biochemistry, and [§]California NanoSystems Institute, University of California, Los Angeles

ABSTRACT We used a multifunctional mesoporous silica nanoparticle (MSNP) carrier to overcome doxorubicin (Dox) resistance in a multidrug resistant (MDR) human breast cancer xenograft by codelivering Dox and siRNA that targets the P-glycoprotein (Pgp) drug exporter. The Pgp siRNA selection from among a series of drug resistance targets was achieved by performing high throughput screening in a MDR breast cancer cell line, MCF-7/MDR. Following the establishment of a MCF-7/MDR xenograft model in nude mice, we demonstrated that a 50 nm MSNP, functionalized by a polyethyleneimine—polyethylene glycol (PEI-PEG) copolymer, provides protected delivery of stably bound Dox and Pgp siRNA to the tumor site. The effective biodistribution and reduced reticuloendothelial uptake, as a result of our nanocarrier design, allowed us to achieve an 8% enhanced permeability and retention effect at the tumor site. Compared to free Dox or the carrier loaded with either drug or siRNA alone, the dual delivery system resulted in synergistic inhibition of tumor growth *in vivo*. Analysis of multiple xenograft biopsies demonstrated significant Pgp knockdown at heterogeneous tumor sites that correspond to the regions where Dox was released intracellularly and induced apoptosis. We emphasize that the heterogeneity originates in the tumor microenvironment, which influences the vascular access, rather than heterogeneous Pgp expression in the MDR cells. Taken together, these data provide proof-of-principle testing of the use of a dual drug/siRNA nanocarrier to overcome Dox resistance in a xenograft. The study also provides the first detailed analysis of the impact of heterogeneity in the tumor microenvironment on the efficacy of siRNA delivery *in vivo*.

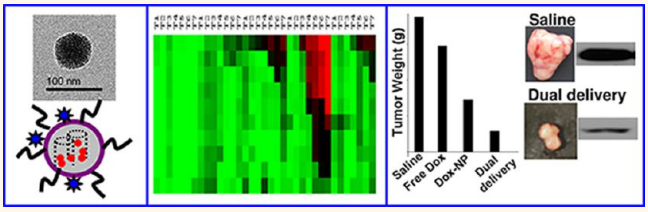

KEYWORDS: multidrug resistance · codelivery · mesoporous silica nanoparticle · high throughput screening · heterogeneous gene knockdown

Although a combination of chemotherapeutic agents are often used to prevent drug resistance in cancer patients, the ability of the cancer cells to adapt and develop one or more drug resistance pathways ultimately leads to treatment failure in most cancers.[1,2] A novel approach to address cancer drug resistance is to take advantage of the ability of nanocarriers to sidestep drug resistance mechanisms by the endosomal delivery of chemotherapeutic agents.[2,3] An additional advantage of nanocarriers is the capability of delivering nucleic acids (*e.g.*, siRNA), which provides the opportunity of knocking down genes involved in drug resistance.[2,4−12] In this regard, we have demonstrated that encapsulation of doxorubicin (Dox) by mesoporous silica nanoparticles (MSNPs) could restore Dox sensitivity in a drug resistant squamous carcinoma cell line by codelivery of a siRNA that knocks down a drug resistance gene.[6] However, drug resistance at the tumor level is complicated, often involving multiple and dynamically acquired multidrug resistance (MDR) mechanisms as a result of the expression of drug efflux pumps (*e.g.*, P-glycoprotein, Pgp or MDR1; multidrug resistance protein, MRP1; breast cancer resistance protein, BCRP or ABCG2),[10,11] antiapoptotic proteins (*e.g.*,

* Address correspondence to hmeng@mednet.ucla.edu.

Received for review July 12, 2012 and accepted December 23, 2012.

Published online January 04, 2013
10.1021/nn3044066

Bcl-2),[13] oncogenes (*e.g.*, c-Myc),[12,14] and regulators of drug metabolism (*e.g.*, pregnane X receptor, PXR).[15,16]

We developed a MSNP platform that is capable of delivering siRNAs that target each of the above resistance mechanisms. To select the most optimal siRNA for knocking down a Dox resistance gene in a xenograft established from a MDR breast cancer cell line (MCF-7), we performed *ex vivo* screening with a 50 nm MSNP platform that was specifically designed for optimal biodistribution and passive delivery at the tumor site following intravenous injection. The cationic surface of the polyethyleneimine-polyethylene glycol (PEI-PEG)-coated particles was used for the attachment of a series of siRNAs, which was subsequently used in a high throughput screening assay to find the most optimal siRNA/drug combination for overcoming Dox resistance in MCF-7/MDR cells. This was accomplished by electrostatic attachment of siRNAs to the MSNP surface, which allows stable and protected siRNA delivery in tissue culture as well as the blood circulation of tumor-bearing animals following intravenous administration. The phosphonate-coated particle pores allow electrostatic Dox attachment and subsequent release by protons in an acidifying endosomal environment.[6] Following the demonstration that codelivery of P-glycoprotein (Pgp) siRNA shows the best Dox synergy *in vitro*, we also sought *in vivo* proof-of-principle testing with the same siRNA/drug combination in a MCF-7/MDR xenograft model in nude mice. While successful, the *in vivo* synergy was affected by the heterogeneity in the tumor microenvironment and vascular access, with effective cell killing only at sites where the dual Dox/Pgp siRNA combination was delivered intracellularly. To our knowledge, this is the first demonstration of the importance of tumor heterogeneity in determining the outcome of siRNA delivery by a nanocarrier.

RESULTS

***Ex Vivo* Screening to Determine the Optimal siRNA Species to Overcome Dox Resistance in a MDR Breast Cancer Cell Line.** MCF-7 cells were used for induction of MDR by exposure to a cocktail of drugs (doxorubicin, daunorubicin, and vinblastine) for 9 weeks. Through the use of a limiting dilution protocol to select single cell clones, we were able to obtain a doxorubicin-resistant clone, MCF-7/MDR, with a Dox IC_{50} of 27.1 μg/mL compared to 4.1 μg/mL in the parental cell line (Supporting Information, Figure S1A). This clone maintained stable Pgp expression in all the progeny in the tissue culture dish, as demonstrated by cells with a single peak of Pgp expression and a uniform reduction in Dox content seen during flow cytometry analysis (Supporting Information, Figure S1B). The MCF-7/MDR clone was subsequently used to select the best possible gene candidate for overcoming Dox resistance from among a panel of siRNAs (Table 1). This panel is representative

TABLE 1. siRNA Panel for Targeting Multiple Drug Resistance Genes in MCF-7 Cells

siRNA species	MDR mechanism and target
Pgp	ABC drug efflux transporter[10,11]
MRP1	ABC drug efflux transporter[44]
ABCG2	ABC drug efflux transporter[45]
Bcl2	antiapoptotic protein[13]
cMyc	oncogene involved in MDR[12]
PXR	expression of the regulator of drug-metabolizing enzymes[46]

of the six major drug resistance pathways that have been elucidated in breast cancer (Table 1). These siRNAs were delivered by a 50 nm particle that was coated with a PEI (1.8 kD)−PEG (5 kD) copolymer and contains an anionic phosphonate-coated surface for electrostatic attachment of Dox as well as PEI.[6,17] Particle design and characterization, including drug and siRNA loading, cellular uptake, subcellular localization, as well as elucidating drug, and siRNA release from an acidifying endosomal compartment are described in the Supporting Information, S2.

The *in vitro* effectiveness of the siRNAs to overcome Dox resistance was tested in a MTS assay that was carried out in MCF-7/MDR cells in 384 well plates, using automated robotic equipment. The high throughput screening (HTS) procedure was carried out at a MSNP dose range of 0.2−100 μg/mL, which is equivalent to a siRNA dose range of 0.002−1 μg/mL and a Dox dose of 0.0066−3.3 μg/mL. Seven different time points over a 3−72 h observation period was used for screening, and the data were displayed as a heatmap, with red indicating robust cell killing while green reflects absence of toxicity (Figure 1A). The cytotoxicity ranking demonstrated that Pgp knockdown provided the best cell killing by Dox, while siRNAs targeting MRP1, ABCG2, Bcl2, cMyc, or PXR had a lesser effect (Figure 1A). This outcome was corroborated by the increased number and intensity of Dox-stained nuclei (red fluorescence) in cells receiving codelivered Pgp siRNA compared to cells treated with free drug or particles delivering Dox without siRNA (Figure 1B). The data are quantitatively expressed in the bar graph on the right-hand side of the figure to demonstrate the synergy between Dox and Pgp siRNA. No significant killing was obtained when cells were treated with MSNP loaded with Pgp siRNA alone (Supporting Information, S3). Pgp knockdown was confirmed by immunoblotting, which demonstrated >50% decrease of protein expression compared to the negligible effect observed for scrambled siRNA (Figure 1C). Assessment of gene knockdown at different time points demonstrated that Pgp siRNA delivery by MSNP in MCF-7/MDR cells achieved maximum gene knockdown <48 h and that this effect lasted for at least 96 h. Incubation of the same carrier in the artificial lysosomal fluid showed steady and continuous Dox release *via* interference of electrostatic

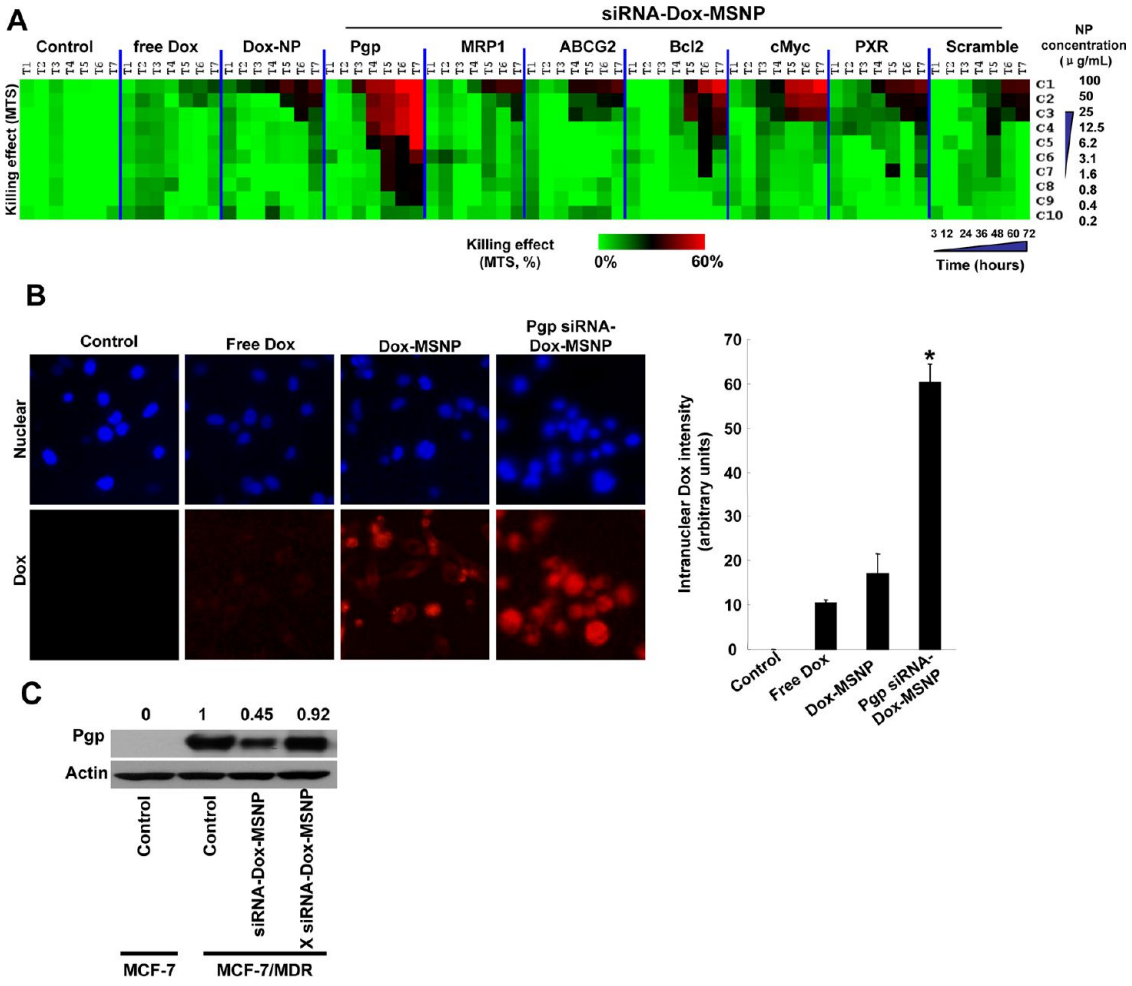

Figure 1. Determination of the optimal Dox/siRNA combination to overcome drug resistance in MCF-7/MDR cells. (A) Heat map display of the HTS cytotoxicity assays were carried out using the MTS reagent in 384-well plates. The data were quantitatively expressed using MeV software to generate heat maps, in which each of the rows and columns represent dose range (C1−C10) and exposure times (T1−T7), respectively. A green color indicates lack of cytotoxicity, while red indicates a significant killing effect. (B) Representative fluorescent images of the cells treated with 100 μg/mL of the Dox-MSNP and Pgp siRNA-Dox-MSNP and free drug for 72 h before Hoechst staining for 0.5 h. Because no washing was performed before imaging, MetaXpress software was used to adjust the background according to the fluorescence intensity of the intranuclear Dox, using the Hoechst to define the nuclear boundary. We also used MetaXpress and Image J software to quantitatively express Dox fluorescence in the different treatment groups, as demonstrated by the graph on the right-hand side. This demonstrated that there is indeed synergy between the drug and Pgp siRNA, as judged by the intensity of intranuclear Dox staining in MCF-7/MDR cells. (C) Immunoblotting was used to measure the Pgp expression after 72 h of treatment with 125 ng/mL Pgp siRNA attached to loaded particles (introduced at a particle dose of 12.5 μg/mL).

drug binding to phosphonate groups on the interior surface of the particle by protons (Supporting Information, S2). The sustained Dox release phase lasted more than 96 h. All considered, the kinetics of Pgp knockdown and the overlap with sustained Dox release allows a synergy that would not be possible by a particle providing burst release of the drug. The key question therefore became whether the synergistic Dox/Pgp siRNA combination is also efficacious in overcoming drug resistance *in vivo*.

Co-delivery of Dox and Pgp siRNA Leads to Synergistic Inhibition at Heterogeneous MCF-7/MDR Tumor Sites in a Mouse Xenograft Model. To demonstrate the potential of Pgp siRNA to knock down gene expression and inhibit tumor growth *in vivo*, MCF-7/MDR cells were grown as xenografts in nude mice. The drug resistance phenotype of the MDR tumor model was confirmed in a preliminary *in vivo* experiment in which free Dox treatment was used to assess the effect on tumor growth in the parental and MCF-7/MDR xenografts (Supporting Information, Figure S4A). This demonstrated that while the free drug could suppress tumor weight gain in xenografts established from the parental cell line by ~90%, there was a significantly lesser (~7%) effect on the MCF-7/MDR xenografts (Figure S4A). Moreover, Pgp overexpression in the MDR xenograft was maintained for a minimal time period of 5 weeks as determined by immunoblotting (Figure S4B). The tumor-bearing nude mice were subsequently injected i.v. with Dox and Pgp-loaded MSNP every 3−6 days for 30 days (Figure 2A). Each animal received a particle dose of 121 mg/kg (Dox, 4 mg/kg; siRNA, 1.2 mg/kg), during each

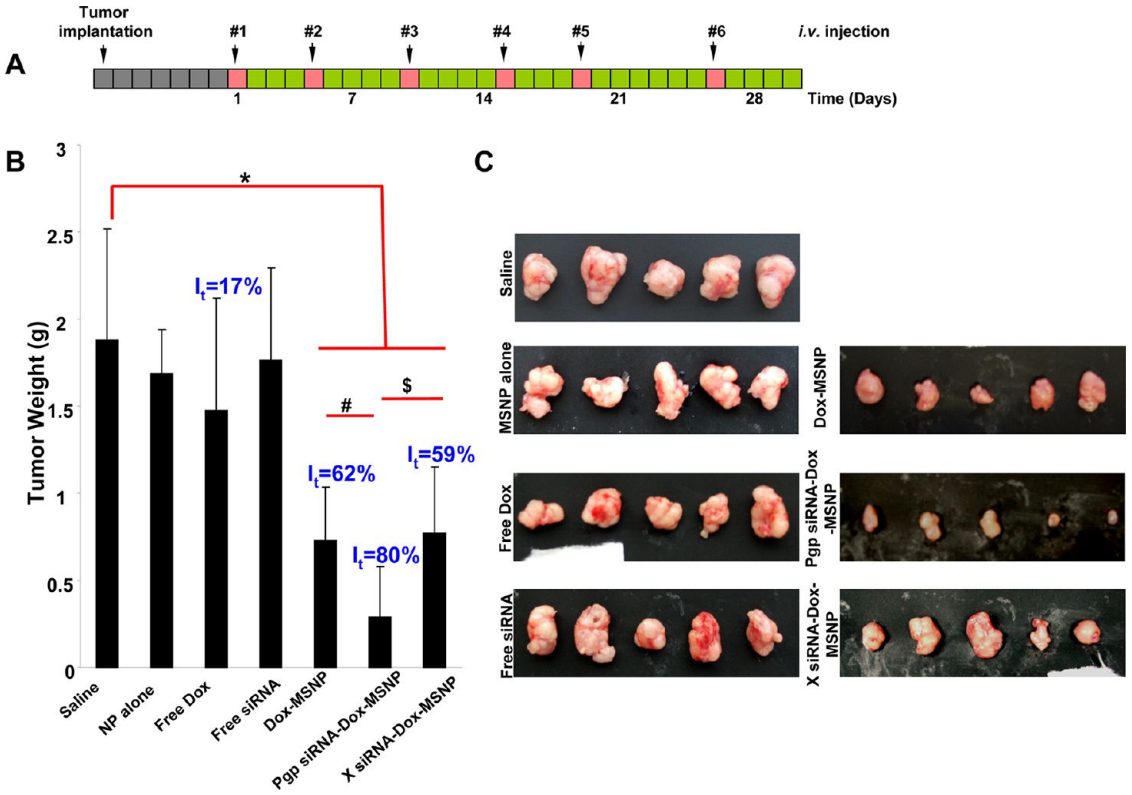

Figure 2. Tumor growth inhibition of xenografts established from MCF-7/MDR cells in nude mice. (A) MCF-7/MDR cancer cells were subcutaneously injected into mice 7 days before treatment with MSNP (gray boxes). These animals received six i.v. injections (red boxes) every 3−6 days (green boxes) for 30 days as shown. (B) Comparison of the tumor inhibition effect of Dox-loaded MSNP containing Pgp siRNA *versus* other treatment groups: saline, empty MSNP, free Dox, free siRNA, Dox-loaded MSNP without siRNA, and Dox-loaded MSNP containing scrambled siRNA. The effect of Pgp siRNA MSNP without Dox is shown in Supporting Information, Figure S3. Following sacrifice of the animals, tumor tissues were collected and weighed to determine the tumor inhibition rate (I_t). (∗) $p < 0.05$, compared to saline; (#) $p < 0.05$, compared to Dox-loaded MSNP without siRNA; ($) $p < 0.05$, compared to Dox-loaded MSNP with scramble (×) siRNA. (C) Photograph of the collected tumor tissues for each treatment group.

injection (Figure 2A). The controls included animals injected with free Dox and Dox-MSNP only. The monodispersed, PEI−PEG decorated particles showed decreased reticuloendothelial system (RES) uptake and resulted in the retention of ~8% of the administered particle dose at the tumor site. The design details for obtaining an optimal biodistribution and enhanced permeability and retention (EPR) effects are discussed in the Supporting Information (Figure S5).

Following sacrifice of the mice after 30 days, we demonstrated that Pgp siRNA-Dox-MSNP showed a significantly higher rate of tumor inhibition (I_t), *i.e.*, 80%, compared to free Dox (I_t = 17%), particles loaded with Dox only (I_t = 62%), or drug-loaded particles with scrambled siRNA (I_t = 59%) (Figure 2B,C and Supporting Information, Figure S6). We did not observe any tumor inhibition in mice receiving injection of Pgp-siRNA-MSNP only. This provides proof-of-principal testing that siRNA targeting can be used to restore Dox sensitivity in a MDR xenograft *in vivo*. A key question therefore became whether the synergistic effect of siRNA is a result of Pgp knockdown *in vivo*.

To demonstrate the role of Pgp knockdown in the interference in tumor growth, it was necessary to study *in situ* cellular killing in relation to Pgp expression in the tumor. This assessment could be conveniently done by using the intense red fluorescence staining of apoptotic nuclei by Dox as well as immunohistochemistry (IHC) to assess Pgp expression. When analyzing multiple tumor sections for each xenograft, we observed clear evidence of a heterogeneous tumor cell killing effect as demonstrated by the Dox-stained apoptotic nuclei in regions where the Pgp was knocked down (Figure 3). Compared to the comparative lack of apoptotic nuclei in animals receiving Dox alone (Figure 3A-2) or Dox-MSNP (Figure 3A-3), there was a significantly higher Dox uptake and cellular apoptosis in tumors of animals treated with Pgp siRNA-Dox-MSNP (Figure 3A-4). This finding is further illustrated by the higher magnification images in Figure 3B, showing the expansion of the regions labeled as "i", "ii", and "iii" in Figure 3A. Figure 3B also shows the parallel nuclear staining with Hoechst, as well as FITC-labeled blood vessels, stained with anti-CD31. The merged panel on the bottom right demonstrates that Dox-stained nuclei colocalize with the Hoechst-stained nuclei and these nuclei were distinguishable from weak or unstained nuclei in an adjacent region. In contrast, tumors from animals treated

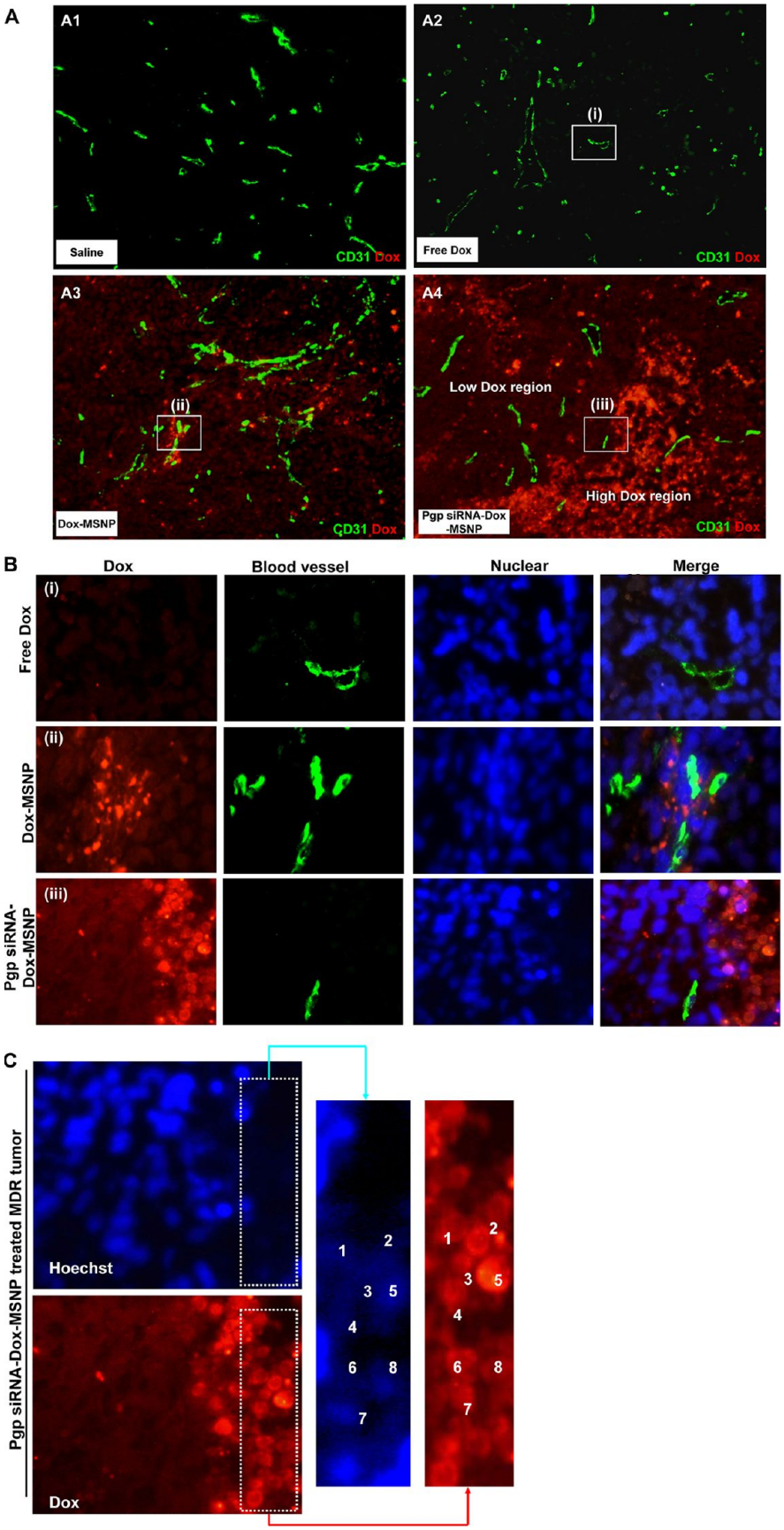

Figure 3. Analysis of intratumoral Dox distribution in the various treatment groups. (A) Dual color fluorescence to show the tumor localization of Dox in relation to the tumor blood vessels, stained for CD31. Part of the tumor tissue from the saline (A1),

continued

free Dox (A2), Dox-MSNP (A3), and Pgp siRNA-Dox-MSNP (A4) groups were frozen and embedded. The sections were incubated with anti-CD31 primary antibody and visualized by a FITC-conjugated secondary antibody. Dox fluorescence (red) was also assessed on the same slide view and merged images were prepared to show drug distribution in relation to the blood vessels. Slides were visualized under a fluorescence microscope at 100× (Zeiss, Germany). (B) Higher magnification images of regions "i", "ii", and "iii" (representing the groups shown in Figure 3A) were obtained after Hoechst staining to demonstrate the nuclear localization in relation to Dox fluorescence in the tumor. (C) Demonstration of colocalization of faint Hoechst-stained with Dox-stained nuclei in the Pgp siRNA-Dox-MSNP treated MDR tumor in Figure 3B-iii. Owing to the cytotoxic effects of Dox and the accompanying nuclear damage, it was not always possible to observe Hoechst staining at the resolution shown in Figure 3B-iii (far right panel). However, image analysis at a higher magnification, demonstrated that it is possible to demonstrate colocalization of faint Hoechst-stained with Dox-stained nuclei.

with Dox-MSNP alone demonstrated a perinuclear distribution of the Dox-loaded particles, with limited nuclear apoptosis (Figure 3B, middle panel). Owing to the cytotoxic effects of Dox and the accompanying nuclear damage, it was not always possible to observe Hoechst staining at the resolution shown in Figure 3B-iii (far right panel). However, image analysis at a higher magnification demonstrated that it is possible to demonstrate colocalization of faint Hoechst-stained with Dox-stained nuclei (Figure 3C).

To understand the difference between low and high Dox-stained regions (Figure 3A-4), we asked whether there are differences in Pgp expression in these sites. To assess this, contiguous tumor sections from Pgp siRNA-Dox-MSNP treated animals were used for CD31 (cyan color) and Pgp staining (green fluorescence) to compare to the distribution of the Dox-stained apoptotic nuclei. This allowed comparison of the abundance and distribution of Dox *versus* Pgp expression in relation to the blood vessels in the tumor (Figure 4A). Merging of red and green fluorescent images demonstrated the differential distribution of Pgp and Dox in the tumor, with the highest Dox-staining coincided with the regions showing the lesser Pgp staining (Figure 4A). We used Image J software to quantify the Pgp expression and Dox content in the three representative areas. This demonstrates that Dox content increases as Pgp expression declines and *vice versa* (Figure 4A, bottom left). Since there is no obvious heterogeneity in Pgp expression in MCF-7/MDR xenografts from nontreated animals (Supporting Information, Figure S7), the heterogeneity that emerges after dual cargo delivery suggests that the tumor microenvironment impacts nanocarrier delivery. One possibility is an effect on vascular access due to the influence of the tumor stroma and extent of pericyte coverage. To our knowledge, this is the first comprehensive demonstration of the contribution of heterogeneity in the tumor environment to determining the efficacy of gene knockdown by a nanocarrier.

Further evidence for heterogeneous gene knockdown was confirmed by Pgp immunoblotting, using multiple randomly selected biopsies from each xenograft. In the example demonstrated in Figure 4B the reduction in Pgp expression ranged from 10 to 90% (average of 47% ± 25%) for the biopsy series labeled S1−S9. We also used IHC and immunoblotting to rule out heterogeneous Pgp expression in tumor tissue from untreated animals (Supporting Information, Figure S7). Statistical analysis of the magnitude of Pgp knockdown was performed by randomly selecting three nonadjacent biopsies sites in each tumor sample (Figure 2C) for immunoblotting and qPCR analysis (labeled as S1−S3 in Figure 5). Integration of all the data demonstrated statistically lower Pgp expression (~50%) in the tumor from Pgp siRNA-Dox-MSNP treated animals compared to saline controls. No significant reduction of Pgp expression in the MCF-7/MDR matrix was seen in the groups treated with free siRNA or Dox-loaded MSNP containing scrambled siRNA (Figure 5B, upper panel). Expression of the data on a scatter plot confirmed the heterogeneous but significant gene knockdown effects at regional sites in the MDR tumors (Figure 5B, lower panel). This trend was confirmed by quantifying Pgp mRNA expression (Figure 5C). Thus, qPCR analysis demonstrated that treatment with Pgp siRNA-Dox-MSNP leads to ~70% reduction in mRNA expression compared to other treatment groups.

Dual delivery of Dox and siRNA Reduces the Systemic and Cardiovascular Side Effects of Dox. Overcoming chemotherapy side effects is an important consideration for drug delivery by nanocarriers.[18] To assess the therapeutic advantage of our MSNP platform, we compared the body weight, blood chemistry, histology, as well as cardiotoxic effects of Dox for the different treatment strategies.[19,20] Thus, animals receiving free Dox showed a significant lower body weight for the entire duration of treatment (Figure 6A). In contrast, animals receiving Dox-MSNP or Pgp siRNA-Dox-MSNP did not show a significant reduction in body weight compared to the saline control. Similar observations were made when comparing the effects on liver function, for which free Dox-treated animals showed a significant elevation of aspartate aminotransferase (AST) levels, which was significantly reduced when the same Dox amount was delivered by MSNP nanocarriers (Supporting Information S8). Use of troponin T (cTnT) levels in the serum, demonstrated a significant increase in the levels of this cardiotoxicity marker in response to free Dox treatment.[19,20] This effect was totally reversed by encapsulating Dox in MSNP (Figure 6B). Finally, histological examination of major organs did not show any gross pathology in any of the treatment groups (Supporting Information S9).

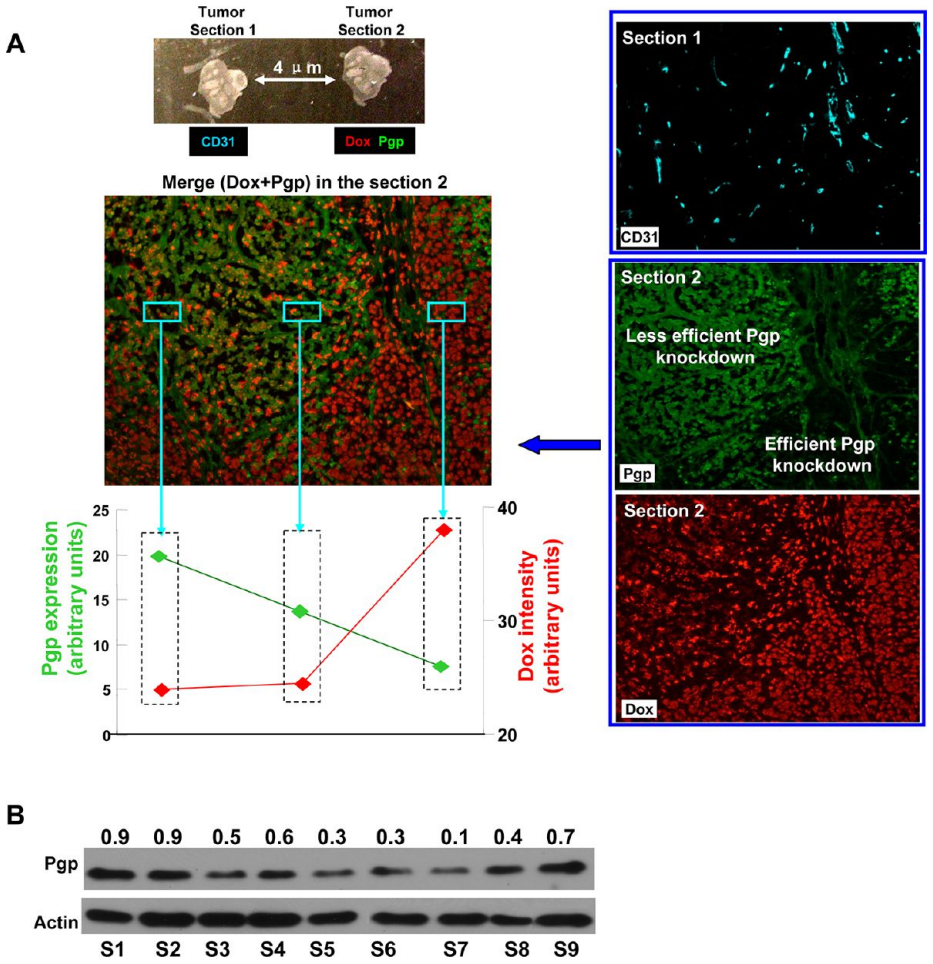

Figure 4. Pgp siRNA-Dox-MSNP treatment leads to heterogeneous effects on cytotoxicity and Pgp expression. (A) To determine whether tumor regions with high and low Dox staining intensity are due to the heterogeneous Pgp knockdown, adjacent sections (4 μm separation) were prepared from this treatment group. The first section was used for CD31 IHC staining (cyan). The second section was used for Pgp staining (green) as well as intratumoral Dox (red) visualization. We also provided merging of the image showing Pgp expression and intratumoral Dox localization in apoptotic nuclei. To quantitatively demonstrate the contrasting distribution of intratumoral Dox and Pgp expression in the dual delivery group, we use Image J software to analyze the Pgp expression and Dox content in three representative areas. As the figure and the Image J analysis show, Dox content clearly tended to increase while Pgp expression decreased and *vice versa*. (B) Immunoblotting analysis to show Pgp expression in randomly selected and nonoverlapping tumor biopsy sites (labeled as "S1→S9") collected from the same tumor xenograft treated with Pgp siRNA-Dox-MSNP.

DISCUSSION

In this study, we demonstrate the use of a multifunctional MSNP carrier to overcome Dox resistance in a MDR human breast cancer xenograft by codelivering Dox with Pgp siRNA. This siRNA was selected from a panel of siRNAs in a HTS assay that was used to compare the most important drug resistance pathways in a MDR breast cancer cell line. Following the establishment of a MDR xenograft from the same cell line in nude mice, we demonstrated that 50 nm MSNPs, functionalized by PEI-PEG copolymers, provides protected delivery of attached Dox and Pgp siRNA to the tumor site. This particle was designed to reduce RES uptake and improve biodistribution, resulting in the retention of ~8% of the injected dose at the tumor site. Compared to drug-only loaded particles, the dual delivery system could achieve synergistic inhibition of tumor growth *in vivo*. Analysis of multiple biopsies in the same tumor demonstrated significant Pgp knockdown at heterogeneous tumor sites, which also corresponded to the regions where nuclear Dox access was associated with the induction of apoptosis. Dox encapsulation by MSNP was associated with reduction in systemic side effects, including reduction of Dox-induced cardiotoxicity. These data demonstrate the feasibility of using a dual drug and siRNA carrier to overcome Dox resistance at the cellular level and *in vivo*. However, our study also showed the negative impact of tumor heterogeneity on the extent of gene knockdown and the necessity to consider the implications of this effect in developing dual nanocarrier therapy.

The feasibility of a nanocarrier overcoming drug resistance through dual drug/siRNA delivery has been demonstrated at the cellular level by a number of

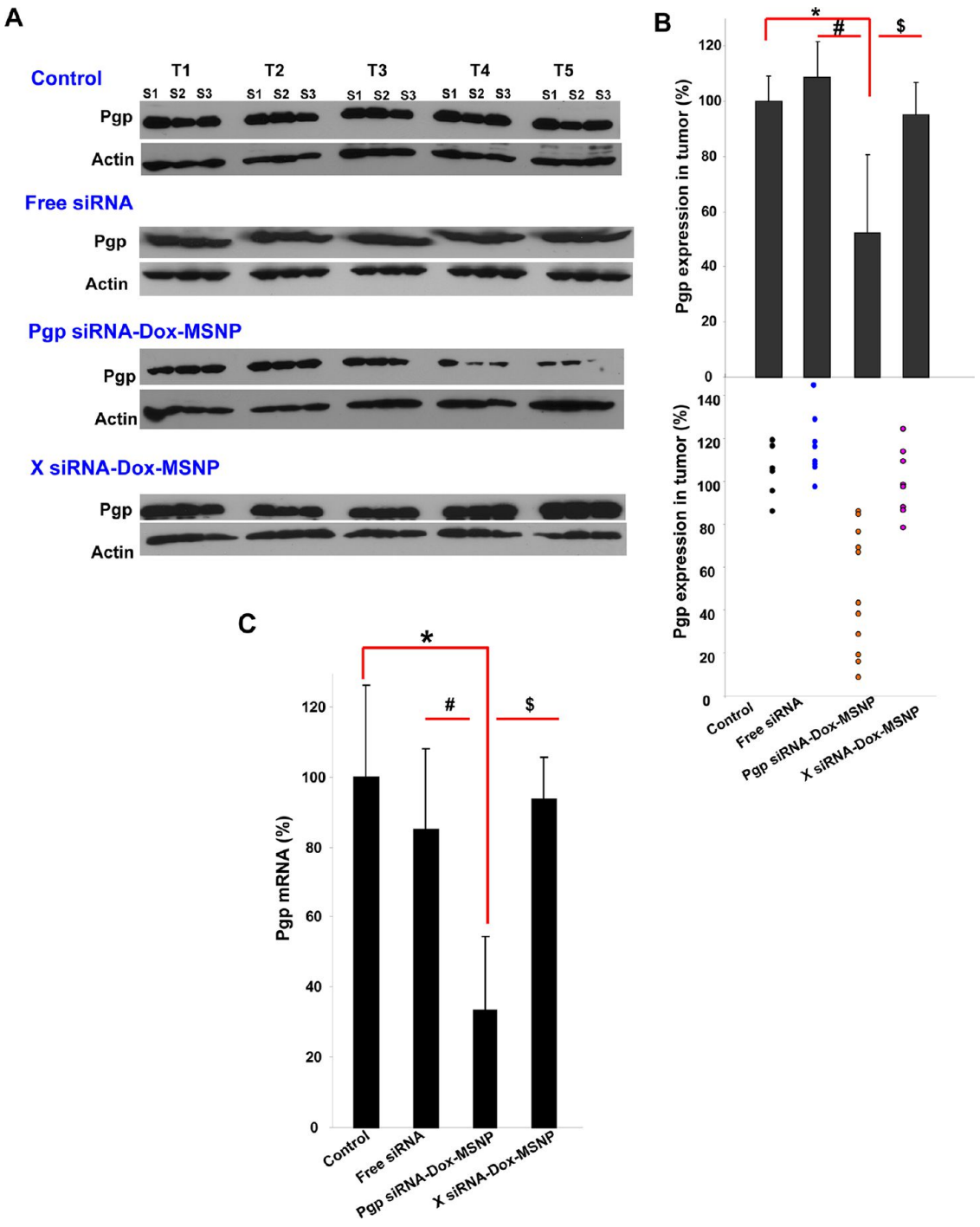

Figure 5. Assessment of Pgp knockdown in the tumors using Western blotting and qPCR. (A) Pgp expression was studied in the different treatment groups using an IHC approach. Randomly selected biopsies taken from three sites in each tumor were used for the analysis (labeled as "S1→S3"). (B) Relative Pgp expression was calculated according to the signal intensities of the protein bands. The data were expressed as a scatter diagram to confirm a significant and heterogeneous knockdown effect in the tumor. (C) At the mRNA level, three randomly selected biopsies per tumor were used for qPCR analysis that was used to confirm the Pgp knockdown effect in the different groups. (*) $p < 0.05$, compared to saline; (#) $p < 0.05$, compared to free Pgp siRNA; ($) $p < 0.05$, compared to Dox-laden MSNP with scramble (×) siRNA.

groups, including our own.[4−7,21−26] This includes the demonstration of siRNA codelivery to silence MDR genes, such as Pgp and Bcl-2, and achieve synergistic cytotoxicity.[4,6,7] However, several of the studies were performed *in vitro* only, or when tested *in vivo*, were performed with different carriers or different administration routes. Moreover, the distribution and heterogeneity of Pgp knockdown across the tumor matrix was not assessed in a detailed fashion, as in the current study. A summary of those data appears in Table S11 in the Supporting Information. Our study is novel from the perspective of the carrier design and studying the

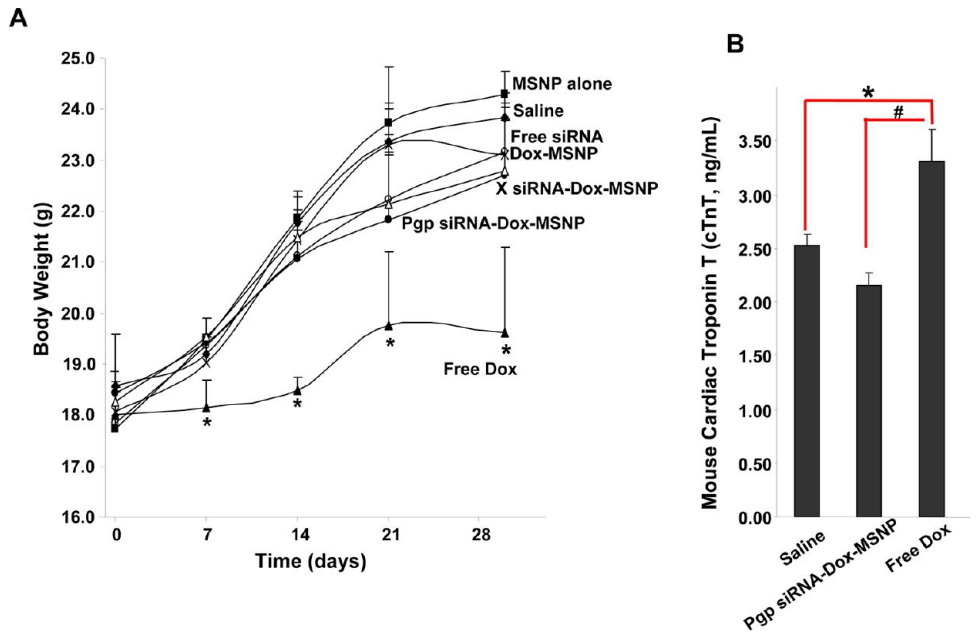

Figure 6. Assessment of the effect of different treatments on animal weight and cTnT levels in the serum. (A) The animal weights were recorded once per week and expressed over the 30 day observation. (B) Serum samples from the different treatment groups were used for cTnT measurement using a commercially available ELISA kit according the manufacture's instruction. (*) $p < 0.05$, compared to saline; (#) $p < 0.05$, compared to free Dox.

in situ distribution of the nanocarrier and Pgp knockdown at the tumor site. While providing proof-of-principle for the concept of dual drug and siRNA delivery, we show the importance of further design features to improve vascular access and improving intratumoral distribution. It may also be necessary to approach nanocancer delivery from the perspective of stratifying cancers based on their vascularity and stromal effects. Thus, additional work is required before dual therapy can be considered as a cancer cure. For this reason, we did not attempt to obtain survival data in the current study.

Owing to the capacity of protected delivery of drug and siRNA compounds, we developed a series of MSNP carriers to attempt to overcome Dox resistance by delivering a range of siRNAs. Clinical drug resistance is dynamic and can be divided into two major categories from the perspective of breast cancer, namely pump and nonpump resistance mechanisms.[1] Pump-related resistance mainly refers to inducible efflux pumps in the cell membrane (*e.g.*, Pgp, MRP1, ABCG2) that actively expel a number of distinct chemotherapeutic agents to decrease the intracellular drug concentration below a cytotoxic threshold.[10,11] The major mechanisms in nonpump resistance refers to the development of genetic and epigenetic alterations that reduce drug sensitivity such as expression of antiapoptotic proteins (*e.g.*, Bcl-2),[13] oncogene expression (*e.g.*, c-Myc),[12,14] and expression of the regulator of drug-metabolizing enzymes (*e.g.*, pregnane X receptor, PXR),[15,16] *etc*. Moreover, the pump and nonpump resistance mechanisms are not mutually exclusive, and can develop in the same cancer cell.[22] We are attempting to address this complexity by using our HTS assay to select the best drug plus siRNA combination for delivery by a nanocarrier designed to optimize biodistribution and retention at the tumor site. The implementation of high throughput or high content screening to assess the effects of siRNA gene knockdown and to assess nanomaterial hazard is increasingly being used in nanotechnology and nanomedicine. From the perspective of dual delivery systems, the screening assisted the selection of an optimal siRNA to combine with Dox, which would otherwise constitute a random choice. Compared to traditional screening to select small molecules, proteins, peptides, and nucleic acids, HTS to optimize the design and therapeutic potential of the nanocarrier requires additional consideration of nanoparticle physicochemical properties, including the contribution of size, shape, rigidity, surface charge, surface coating, type, and amount of payload, *etc*. The potential utility of a HTS approach was also demonstrated in the optimal design of polymeric nanoparticles for the delivery of docetaxel to tumor sites in patients by Hrkach *et al.*[27] In similar fashion, we used an iterative design process and HTS to select the MSNP carrier with optimal size, charge, surface coating, PEI polymer length, pore design, *etc*, to perform dual delivery, reduce RES uptake, prolong the circulation time, and obtain high retention at the xenograft site.[6,17,28]

The heterogeneous gene knockdown effect in our tumor xenografts has been observed previously in cellular siRNA delivery studies, in which nanocarriers have been reported to induce clonal heterogeneity in a

cell population in the same tissue culture dish.[29,30] Minimally, the *in vitro* heterogeneity can be explained by the amount of siRNA being delivered to individual cells, with differences in the cell cycle making an additional contribution.[30] Moreover, considerable intratumor gene heterogeneity has been demonstrated in primary epithelial breast carcinomas prior to treatment.[31,32] However, it is unlikely that our use of an immortal breast cancer cell line will explain the heterogeneity of Pgp expression in our samples, as demonstrated by immunoblotting and IHC (Supporting Information S7). A more likely explanation for the varied Pgp expression and cytotoxicity in our study is the heterogeneous distribution of the MSNPs as a result of differences in the vascularity and vascular access, for example, the extent of pericyte coverage and influence of the tumor stroma.[33,34] While it is outside of the scope of the current study, it is reasonable to postulate that the nucleic acid and drug delivery can be improved by addressing intratumor distribution. One option could be to reduce particle size, but this comes at the expense of lowering the loading capacity of the carrier. Design of an active delivery system that includes targeting ligands (*e.g.*, transferrin, folic acid) could improve particle distribution as well as particle retention in the tumor tissue.[33,35] One might also attempt to manipulate the tumor microenvironment by elevating systemic blood pressure with angiotensis II,[36] using a vasodilator such as an agent that releases NO,[37] small molecule inhibitors of pericyte growth and maturation,[38] or increasing vascular permeability.[34,39]

It is worth pointing out that our MSNP platform is devoid of biohazard, including previous demonstration of its biocompatibility,[17,40] biodegradability,[41] and bioelimination of mesoporous silica.[4,42] In fact, we have recently demonstrated that the intrinsic safety of Stöber and mesoporous silica, which are produced under low temperature synthesis conditions, is due to the absence of high energy, strained 3-member siloxane rings, which are frequently present in high temperature silicas (*e.g.*, quartz and fumed silica) and lead to toxicity due to surface reconstruction and display of H-bonded silanols.[43] We also demonstrate that Dox encapsulation reduces cardiovascular toxicity, which limits the dose of the drug that can be administered.

CONCLUSION

We demonstrate the use of a multifunctional mesoporous silica nanoparticle carrier to overcome Dox resistance in a multidrug resistant human breast cancer xenograft by codelivering Dox and siRNA that targets the P-glycoprotein drug exporter. The Pgp siRNA selection from among a series of drug resistance targets was achieved by performing high throughput screening in a MDR breast cancer cell line. Compared to free Dox or the carrier loaded with either drug or siRNA alone, the systemic administration of Dox and siRNA dual delivery nanoparticle resulted in synergistic inhibition of tumor growth in a MDR tumor xenograft model *in vivo*. We also demonstrated significant Pgp knockdown at heterogeneous tumor sites, which correspond to the regions where Dox was released intracellularly and induced apoptosis. These data provide proof-of-principle testing of the use of dual drug/siRNA MSNP nanocarrier to overcome Dox resistance in a xenograft.

MATERIALS AND METHODS

Materials and Experimental Details. The materials and experimental methods are described in detail in the Supporting Information (S10).

Synthesis and Characterization of MSNP. The synthesis of the 50 nm MSNPs was carried out as previously described by us.[17] The particle surface was further modified using electrostatic attachment of a 1.8 kD PEI polymer, which was used for subsequent covalent attachment of 5 kD PEG. The particles were fully characterized for size distribution, shape, and charge in water, saline, and saline supplemented with 10% mouse serum. The detailed synthesis information was provided in the Supporting Information S10.

Discovery of Optimal Drug/siRNA Combination Using *in Vitro* HTS Assay. The optimal siRNA to be codelivered with Dox was selected by employing a HTS assay. Briefly, MCF-7/MDR cells were plated in 384-well plates. Dox-loaded MSNP, which was sonicated for 15 s before use, was mixed with various siRNAs (Table 1) at particle/siRNA ratio of 100:1. An amount of 25 μL of CDMEM containing Dox alone, empty particles, Dox-MSNP or Dox/siRNA-MSNP were added to the cells. After incubation with the indicated dose of MSNP for various lengths of time at 37 °C, another 25 μL of CDMEM containing Hoechst 33342 nuclear dye at 1 μM was added into each well. Each 384-well plate was incubated for 30 min in the dark. Epifluorescence readings were obtained at the indicate time points using an Image-Xpressmicro (Molecular Devices, Sunnyvale, CA) equipped with a laser autofocus. DAPI and TRITC filters were used to image nuclear (blue fluorescence) and intracellular Dox (red fluorescence). The same plates were also used for assessing cellular viability using the MTS reagent. The mean absorbance of nonexposed cells served as the reference for calculating 100% cellular viability.

Assessment of Dual Delivery in MCF-7/MDR Tumor Xenograft. MCF-7/MDR tumor-bearing mice were randomly divided into seven groups, each of which contained five animals per group, to compare the effects of saline, empty MSNP, free Dox, free siRNA, Dox-loaded MSNP, Dox-siRNA MSNP, and Dox-loaded particles containing scrambled siRNA. The Pgp siRNA-Dox-MSNP group received i.v. administration of a particle dose of 120 mg/kg (~2.4 mg per animal), which is equivalent to a Dox dose of 4 mg/kg (~0.08 mg per animal) and siRNA dose of 1.2 mg/kg (~0.024 mg per animal) per injection. The injections were repeated six times over a 30 day period. Similar doses of particles, drug, and siRNA were injected in the rest of the animal groups over 30 days. Saline was used as negative control. The body weights and tumor sizes were accurately recorded once per week.

Intratumoral Distribution of Dox and Pgp Expression. Tumor tissues from all the treatment groups were frozen and OCT was embedded before continuous sectioning to provide 4 μm thick slices. The first section was used for CD31 IHC staining. The second section was used for Pgp IHC staining and assessment of Dox fluorescence. The experimental details are described in the Supporting Information section S10.

Immunoblotting and qPCR Analysis. To view Pgp and actin expression, multiple random biopsies obtained from each tumor

were lysed in a lysis buffer, electrophoresed on 4−12% gradient SDS-PAGE (Invitrogen, Grand Island, NY) and transferred to a PVDF membrane. After blocking of the membranes, these were overlaid with primary and secondary antibodies, and the blots were developed using the ECL reagent. The immunoblotting data were also confirmed by qPCR analysis. Tumor tissues were harvested, randomly spliced into 2−3 sections, and separately placed in 1 mL of Trizol reagent. The cDNA product was added to a mixture of iQ SYBR Green Supermix (Bio-Rad Laboratories) along with Pgp forward and reverse primers (5′-AGG AAG CCA ATG CCT ATG ACT TTA-3′ and 5′-CAA CTG GGC CCC TCT CTC TC-3′, respectively). The PCR was run at 95 °C for 10 min, followed by 40 cycles at 95 °C for 15 s and 60 °C for 1 min. The relative gene expression was analyzed using Ct method and normalized using β-actin as an endogenous control.

Blood Biochemistry, Tumor, and Major Organ Histology, and cTnT Assay. Mice were sacrificed and serum, tumor, liver, kidney, spleen, lung, heart, and brain were collected for blood biochemistry and histological analysis in the UCLA Division of Laboratory Animal Medicine diagnostic services laboratory. The serum samples were also used for cTnT assay using a commercially available ELISA kit according to the manufacturer's instruction (MyBioSource, San Diego, CA).

Conflict of Interest: The authors declare no competing financial interest.

Acknowledgment. This study was funded by the US Public Health Service Grant RO1 CA133697. We thank Bryan France in Dr. Ken Bradley's laboratory in providing technical assistance of luciferase transfection of cancer cells.

Supporting Information Available: Additional figures, table, results, and method descriptions as described in the text. This material is available free of charge *via* the Internet at http://pubs.acs.org.

REFERENCES AND NOTES

1. Gottesman, M. M. Mechanisms of Cancer Drug Resistance. *Annu. Rev. Med.* **2002**, *53*, 615–662.
2. Jabr-Milane, L. S.; van Vlerken, L. E.; Yadav, S.; Amiji, M. M. Multifunctional Nanocarriers to Overcome Tumor Drug Resistance. *Cancer Treat. Rev.* **2008**, *34*, 592–602.
3. Chow, E. K.; Zhang, X.-Q.; Chen, M.; Lam, R.; Robinson, E.; Huang, H.; Schaffer, D.; Osawa, E.; Goga, A.; Ho, D. Nanodiamond Therapeutic Delivery Agents Mediate Enhanced Chemoresistant Tumor Treatment. *Sci. Transl. Med.* **2011**, *3*, 73ra21.
4. Chen, Y.; Bathula, S. R.; Li, J.; Huang, L. Multifunctional Nanoparticles Delivering Small Interfering RNA and Doxorubicin Overcome Drug Resistance in Cancer. *J. Biol. Chem.* **2010**, *285*, 22639–22650.
5. Patil, Y. B.; Swaminathan, S. K.; Sadhukha, T.; Ma, L.; Panyam, J. The Use of Nanoparticle-Mediated Targeted Gene Silencing and Drug Delivery to Overcome Tumor Drug Resistance. *Biomaterials* **2010**, *31*, 358–365.
6. Meng, H.; Liong, M.; Xia, T.; Li, Z.; Ji, Z.; Zink, J. I.; Nel, A. E. Engineered Design of Mesoporous Silica Nanoparticles to Deliver Doxorubicin and P-Glycoprotein siRNA to Overcome Drug Resistance in a Cancer Cell Line. *ACS Nano* **2010**, *4*, 4539–4550.
7. Alex, M. C.; Min, Z.; Dongguang, W.; Dirk, S.; Oleh, T.; Tamara, M.; Huixin, H. Co-delivery of Doxorubicin and Bcl-2 siRNA by Mesoporous Silica Nanoparticles Enhances the Efficacy of Chemotherapy in Multidrug-Resistant Cancer Cells. *Small* **2009**, *5*, 2673–2677.
8. Liang, X.-J.; Meng, H.; Wang, Y.; He, H.; Meng, J.; Lu, J.; Wang, P. C.; Zhao, Y.; Gao, X.; Sun, B.; *et al.* Metallofullerene Nanoparticles Circumvent Tumor Resistance to Cisplatin by Reactivating Endocytosis. *Proc. Natl. Acad. Sci. U.S.A.* **2010**, *107*, 7449–7454.
9. Shieh, M.-J.; Hsu, C.-Y.; Huang, L.-Y.; Chen, H.-Y.; Huang, F.-H.; Lai, P.-S. Reversal of Doxorubicin-Resistance by Multifunctional Nanoparticles in MCF-7/ADR Cells. *J. Controlled Release* **2010**, *152*, 418–425.
10. Dönmeza, Y.; Gündüz, U. Reversal of Multidrug Resistance by Small Interfering RNA (siRNA) in Doxorubicin-Resistant MCF-7 Breast Cancer Cells. *Biomed. Pharmacother.* **2011**, *65*, 85–89.
11. Wu, H.; Hait, W. N.; Yang, J.-M. Small Interfering RNA-induced Suppression of MDR1 (P-Glycoprotein) Restores Sensitivity to Multidrug-Resistant Cancer Cells. *Cancer Res.* **2003**, *63*, 1515–1519.
12. Kim, D.-Y.; Kim, M.-J.; Kim, H.-B.; Lee, J.-W.; Bae, J.-H.; Kim, D.-W.; Kang, C.-D.; Kim, S.-H. Suppression of Multidrug Resistance by Treatment with TRAIL in Human Ovarian and Breast Cancer Cells with High Level of c-Myc. *Biochim. Biophys. Acta* **2011**, *1812*, 796–805.
13. Lima, R. T.; Martins, L. M.; Guimaraes, J. E.; Sambade, C.; Vasconcelos, M. H. Specific Downregulation of Bcl-2 and xIAP by RNAi Enhances the Effects of Chemotherapeutic Agents in MCF-7 Human Breast Cancer Cells. *Cancer Gene Ther.* **2004**, *11*, 309–316.
14. Chen, J.; Yuan, Y.; Zhang, J.; DY., Z. Up-Regulation of c-myc Expression in MCF-7/Adr Human Breast Cancer Cells and Its Association with Resistance against Doxorubicin. *Di Yi Jun Yi Da Xue Xue Bao* **2002**, *22*, 124–126.
15. Masuyama, H.; Nakatsukasa, H.; Takamoto, N.; Hiramatsu, Y. Down-Regulation of Pregnane X Receptor Contributes to Cell Growth Inhibition and Apoptosis by Anticancer Agents in Endometrial Cancer Cells. *Mol. Pharmacol.* **2007**, *72*, 1045–1053.
16. Sandanaraj, E.; Lal, S.; Selvarajan, V.; Ooi, L. L.; Wong, Z. W.; Wong, N. S.; Ang, P. C. S.; Lee, E. J. D.; Chowbay, B. PXR Pharmacogenetics: Association of Haplotypes with Hepatic CYP3A4 and ABCB1Messenger RNA Expression and Doxorubicin Clearance in Asian Breast Cancer Patients. *Clin. Cancer Res.* **2008**, *14*, 7116–7126.
17. Meng, H.; Xue, M.; Xia, T.; Ji, Z.; Tarn, D. Y.; Zink, J. I.; Nel, A. E. Use of Size and a Copolymer Design Feature To Improve the Biodistribution and the Enhanced Permeability and Retention Effect of Doxorubicin-Loaded Mesoporous Silica Nanoparticles in a Murine Xenograft Tumor Model. *ACS Nano* **2011**, *5*, 4131–4144.
18. Zhang, H.; Ji, Z.; Xia, T.; Meng, H.; Low-Kam, C.; Liu, R.; Pokhrel, S.; Lin, S.; Wang, X.; Liao, Y.-P.; *et al.* Use of Metal Oxide Nanoparticle Band Gap To Develop a Predictive Paradigm for Oxidative Stress and Acute Pulmonary Inflammation. *ACS Nano* **2012**, *6*, 4349–4368.
19. Kismet, E.; Varan, A.; Ayabakan, C.; Alehan, D.; Portakal, O.; Büyükpamukçu, M. Serum Troponin T Levels and Echocardiographic Evaluation in Children Treated with Doxorubicin. *Pediatr. Blood Cancer* **2004**, *42*, 220–224.
20. Herman, E. H.; Lipshultz, S. E.; Rifai, N.; Zhang, J.; Papoian, T.; Yu, Z.-X.; Takeda, K.; Ferrans, V. J. Use of Cardiac Troponin T Levels as an Indicator of Doxorubicin-Induced Cardiotoxicity. *Cancer Res.* **1998**, *58*, 195–197.
21. Sun, T.-M.; Du, J.-Z.; Yao, Y.-D.; Mao, C.-Q.; Dou, S.; Huang, S.-Y.; Zhang, P.-Z.; Leong, K. W.; Song, E.-W.; Wang, J. Simultaneous Delivery of siRNA and Paclitaxel *via* a Two-in-One Micelleplex Promotes Synergistic Tumor Suppression. *ACS Nano* **2011**, *5*, 1483–1494.
22. Saad, M.; Garbuzenko, O. B.; Minko, T. Co-delivery of siRNA and an Anticancer Drug for Treatment of Multidrug-Resistant Cancer. *Nanomedicine* **2008**, *3*, 761–776.
23. Chen, Y.; Wu, J. J.; Huang, L. Nanoparticles Targeted with NGR Motif Deliver c-myc siRNA and Doxorubicin for Anticancer Therapy. *Mol. Ther.* **2010**, *18*, 828–834.
24. Garbuzenko, O. B.; Saad, M.; Pozharov, V. P.; Reuhl, K. R.; Mainelis, G.; Minko, T. Inhibition of Lung Tumor Growth by Complex Pulmonary Delivery of Drugs with Oligonucleotides as Suppressors of Cellular Resistance. *Proc. Natl. Acad. Sci. U.S.A.* **2010**, *107*, 10737–10742.
25. Jiang, J.; Yang, S.-j.; Wang, J.-c.; Yang, L.-j.; Xu, Z.-z.; Yang, T.; Liu, X.-y.; Zhang, Q. Sequential Treatment of Drug-Resistant Tumors with RGD-Modified Liposomes Containing siRNA or Doxorubicin. *Eur. J. Pharm. Biopharm.* **2010**, *76*, 170–178.
26. Tanaka, T.; Mangala, L. S.; Vivas-Mejia, P. E.; Nieves-Alicea, R.; Mann, A. P.; Mora, E.; Han, H.-D.; Shahzad, M. M. K.; Liu, X.; Bhavane, R.; *et al.* Sustained Small Interfering RNA Delivery by Mesoporous Silicon Particles. *Cancer Res.* **2010**, *70*, 3687–3696.
27. Hrkach, J.; Von Hoff, D.; Ali, M. M.; Andrianova, E.; Auer, J.; Campbell, T.; De Witt, D.; Figa, M.; Figueiredo, M.;

Horhota, A.; *et al.* Preclinical Development and Clinical Translation of a PSMA-Targeted Docetaxel Nanoparticle with a Differentiated Pharmacological Profile. *Sci. Transl. Med.* **2012**, *4*, 128ra39.
28. Zhang, H.; Xia, T.; Meng, H.; Xue, M.; George, S.; Ji, Z.; Wang, X.; Liu, R.; Wang, M.; France, B.; *et al.* Differential Expression of Syndecan-1 Mediates Cationic Nanoparticle Toxicity in Undifferentiated *versus* Differentiated Normal Human Bronchial Epithelial Cells. *ACS Nano* **2011**, *5*, 2756–2769.
29. Chen, A. A.; Derfus, A. M.; Khetani, S. R.; Bhatia, S. N. Quantum Dots to Monitor RNAi Delivery and Improve Gene Silencing. *Nucleic Acids Res.* **2005**, *33*, e190.
30. Raab, R. M.; Stephanopoulos, G. Dynamics of Gene Silencing by RNA Interference. *Biotechnol. Bioeng.* **2004**, *88*, 121–132.
31. Wild, P.; Knuechel, R.; Dietmaier, W.; Hofstaedter, F.; Hartmann, A. Laser Microdissection and Microsatellite Analyses of Breast Cancer Reveal a High Degree of Tumor Heterogeneity. *Pathobiology* **2000**, *68*, 180–190.
32. Mariani-Costantini, R.; Escot, C.; Theillet, C.; Gentile, A.; Merlo, G.; Lidereau, R.; Callahan, R. *In Situ* c-myc Expression and Genomic Status of the c-myc Locus in Infiltrating Ductal Carcinomas of the Breast. *Cancer Res.* **1988**, *48*, 199–205.
33. Sanhai, W. R.; Sakamoto, J. H.; Canady, R.; Ferrari, M. Seven Challenges for Nanomedicine. *Nat. Nanotechnol.* **2008**, *3*, 242–244.
34. Sugahara, K. N.; Teesalu, T.; Karmali, P. P.; Kotamraju, V. R.; Agemy, L.; Greenwald, D. R.; Ruoslahti, E. Coadministration of a Tumor-Penetrating Peptide Enhances the Efficacy of Cancer Drugs. *Science* **2010**, *328*, 1031–1035.
35. Ferris, D. P.; Lu, J.; Gothard, C.; Yanes, R.; Thomas, C. R.; Olsen, J.-C.; Stoddart, J. F.; Tamanoi, F.; Zink, J. I. Synthesis of Biomolecule-Modified Mesoporous Silica Nanoparticles for Targeted Hydrophobic Drug Delivery to Cancer Cells. *Small* **2011**, *7*, 1816–1826.
36. Suzuki, M.; Hori, K.; Abe, I.; Saito, S.; Sato, H. A New Approach to Cancer Chemotherapy: Selective Enhancement of Tumor Blood Flow with Angiotensin II. *J. Natl. Cancer Inst.* **1981**, *67*, 663–669.
37. Seki, T.; Fang, J.; Maeda, H. Enhanced Delivery of Macromolecular Antitumor Drugs to Tumors by Nitroglycerin Application. *Cancer Sci.* **2009**, *100*, 2426–2430.
38. Kano, M. R.; Bae, Y.; Iwata, C.; Morishita, Y.; Yashiro, M.; Oka, M.; Fujii, T.; Komuro, A.; Kiyono, K.; Kaminishi, M.; *et al.* Improvement of Cancer-Targeting Therapy, Using Nanocarriers for Intractable Solid Tumors by Inhibition of TGF-beta Signaling. *Proc. Natl. Acad. Sci. U.S.A.* **2007**, *104*, 3460–3465.
39. Minko, T.; Kopečkova, P.; Pozharov, V.; Jensen, K. D.; Kopeček, J. The Influence of Cytotoxicity of Macromolecules and of VEGF Gene Modulated Vascular Permeability on the Enhanced Permeability and Retention Effect in Resistant Solid Tumors. *Pharm. Res.* **2000**, *17*, 505–514.
40. Xia, T.; Kovochich, M.; Liong, M.; Meng, H.; Kabehie, S.; George, S.; Zink, J. I.; Nel, A. E. Polyethyleneimine Coating Enhances the Cellular Uptake of Mesoporous Silica Nanoparticles and Allows Safe Delivery of siRNA and DNA Constructs. *ACS Nano* **2009**, *3*, 3273–3286.
41. Cauda, V.; Schlossbauer, A.; Bein, T. Bio-degradation Study of Colloidal Mesoporous Silica Nanoparticles: Effect of Surface Functionalization with Organo-silanes and Poly(ethylene glycol). *Microporous Mesoporous Mater.* **2010**, *132*, 60–71.
42. Souris, J. S.; Lee, C.-H.; Cheng, S.-H.; Chen, C.-T.; Yang, C.-S.; Ho, J.-a. A.; Mou, C.-Y.; Lo, L.-W. Surface Charge-Mediated Rapid Hepatobiliary Excretion of Mesoporous Silica Nanoparticles. *Biomaterials* **2010**, *31*, 5564–5574.
43. Zhang, H.; Dunphy, D. R.; Jiang, X.; Meng, H.; Sun, B.; Tarn, D.; Xue, M.; Wang, X.; Lin, S.; Ji, Z.; *et al.* Processing Pathway Dependence of Amorphous Silica Nanoparticle Toxicity: colloidal *versus* Pyrolytic. *J. Am. Chem. Soc.* **2012**, *134*, 15790–15804.
44. Zhang, F.; Du, G.; Zhang, L.; Zhang, C.; Lu, W.; Liang, W. Naringenin Enhances the Anti-Tumor Effect of Doxorubicin through Selectively Inhibiting the Activity of Multidrug Resistance-Associated Proteins but not P-glycoprotein. *Pharm. Res.* **2009**, *26*, 914–925.
45. Davies, G. F.; Juurlink, B. H.; Harkness, T. A. Troglitazone Reverses the Multiple Drug Resistance Phenotype in Cancer Cells. *Drug Des. Dev. Ther.* **2009**, *3*, 79–88.
46. Harmsen, S.; Meijerman, I.; Febus, C.; Maas-Bakker, R.; Beijnen, J.; Schellens, J. PXR-Mediated Induction of P-glycoprotein by Anticancer Drugs in a Human Colon Adenocarcinoma-Derived Cell Line. *Cancer Chemoth. Pharm.* **2010**, *66*, 765–771.